

International Journal of Advanced Research in Science, Communication and Technology

International Open-Access, Double-Blind, Peer-Reviewed, Refereed, Multidisciplinary Online Journal

Impact Factor: 7.67

Volume 5, Issue 1, October 2025

Regenerative Braking Control and Energy Recovery Optimization for Brushless DC Motor Electric Vehicles

Ankur Singh¹ and Ashish Bhargava²

M. Tech Scholar, Bhabha Engineering Research Institute, Bhopal, MP¹ Professor, Bhabha Engineering Research Institute, Bhopal, MP²

Abstract: Based on a Brushless DC (BLDC) motor, this research provides a novel regenerative braking approach. The recommended approach for braking involves using a variable Stator voltage from a multicell battery system DC-DC buck converter. To evaluate the performance of the proposed braking system, a simulation was used. According to simulation results, the proposed regenerative braking technique is practical and efficient. Additionally, this research introduces the most fundamental technology for regenerative braking using a BLDC motor to improve the mileage of lightweight electric vehicles (EVs).

Keywords: Solar PV, Electric Vehicle, Regenerative Braking, Zeta Converter, P&O - MPPT, Battery & PMBLDC.

I. INTRODUCTION

The significant environmental risks associated with carbon emissions and the divestment from fossil fuels need the development of alternate or renewable energy sources. The transition from internal combustion engines to electric vehicles is a crucial advancement for humanity in achieving zero carbon emissions and sustainable development. The PMBLDC motor has seen widespread use in light electric vehicle sectors, such as e-rickshaws and two-wheelers, due to its simpler control algorithm compared to other EV motors. During deceleration, energy is efficiently recuperated in a PMBLDC motor and stored in the battery. Electrical braking often proves inefficient at speeds less a certain threshold, and energy recovery is not feasible during emergency braking. Compatibility of electronic and mechanical brakes [1]. The amount of regeneration achievable is contingent upon the braking pressure exerted on the throttle, as seen in [2]. [3] incorporates a fuzzy logic control technology that significantly enhances braking performance. Sliding mode control offers superior steady-state performance, effectively minimizing undesirable oscillations in the DC bus during transitions between driving and braking modes [4]. Utilize a bidirectional DC-DC converter to regulate DC bus voltage and facilitate reverse power flow during braking. The back electromotive force of the motor must remain constant for efficient battery charging [6]. To ascertain rotor position, locate the zero-crossings of the back electromotive force [7]. The rotor location is determined with greater precision by analyzing the inverter switching behavior [8]. The third harmonic stator voltage waveform provides rotor position information and may be used to create a sensor-free method. The zeta converter optimally extracts maximum power from the solar panel while maintaining stable dynamic performance under diverse environmental circumstances. In solar photovoltaic applications, the Zeta converter has distinct benefits compared to other DC-DC converters:

- It can manage a wide range of MPPTs under dynamic settings since it operates in buck-boost mode. [12]. The highest duty ratio of a basic buck or boost converter refers to a certain mode of operation.
- The output inductor of the zeta converter ensures that there is no ripple current at the output of the boost or buck-boost converter [13].
- The zeta converter has noninverted output polarity, as opposed to the Cuk converter, which has both input and
 output ripple free current. As a consequence, negative voltage sensing is no longer required, reducing the
 complexity of sensor circuits. [14].

Copyright to IJARSCT www.ijarsct.co.in







International Journal of Advanced Research in Science, Communication and Technology

International Open-Access, Double-Blind, Peer-Reviewed, Refereed, Multidisciplinary Online Journal

Volume 5, Issue 1, October 2025

Impact Factor: 7.67

Figure 1 illustrates the solar photovoltaic array and the battery-operated permanent magnet brushless DC motor drive. A bidirectional DC-DC converter connects the battery to the DC connection, resulting in increased cost and weight. The bidirectional DC-DC converter manages battery charging and discharging by sustaining the DC connection voltage. A DC-DC power converter is used in the input stage of Maximum Power Point Tracking (MPPT). Two voltage sensors, two current sensors, and Hall effect sensors for positional feedback are necessary for speed regulation. The DC-DC converter in [15] is replaced with a Z-source DC-DC converter. Regulating this kind of DC-DC converter requires intricate control mechanisms, including the supervision of phase currents and DC link voltage.

This is an outline of the paper. Section II delineates the system. Part III delineates the design methodologies. Section IV delineates the used control procedures, followed by the outcomes in Section V and the conclusion in Section VI.

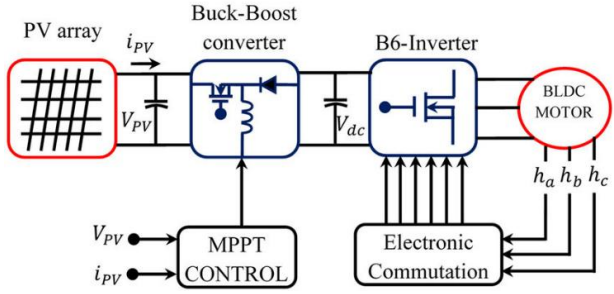


Fig 1:PV-powered BLDC motor driving system block diagram

II. SYSTEM DESCRIPTION AND OPERATION

The vehicle's powertrain consists of a solar panel, a zeta converter, a three-phase voltage source inverter (VSI), and a PMBLDC motor. The proposed solution, by connecting the battery to the system DC bus, obviates the need for an additional power converter and significantly reduces the quantity of sensors required. The suggested system needs just two voltage sensors to facilitate MPPT and sensorless control.

The engine requires power, supplied by the battery and the solar photovoltaic panel. The solar panel's maximum power is sent to the VSI via a zeta converter. An incremental conductance method is used for maximum power point tracking (MPPT) operation. The VSI and the intermediary zeta converter provide the whole electrical power from the DC bus to the load. The P&O-MPPT technique is used by a pulse generator to generate switching pulses for the zeta converter, adjusting the duty ratio to optimize converter performance at maximum power. The predicted duty ratio is then compared to a high-frequency carrier signal to ensure optimal switching efficiency at the greatest optimum power point for the converter. The electrical commutation logic of the PMBLDC motor regulates the switching of the VSI's IGBTs. The VSI operates at the fundamental frequency, resulting in reduced switching losses. Furthermore, energy is reciprocally recycled from both sources to loads. The VSI is now charging the battery and functioning as a rectifier. Position sensor-less control for electronic commutation of the PMBLDC motor is also viable, obviating the need for mechanical Hall sensors and the associated intricate electrical circuitry.

III. MAXIMUM POWER POINT TRACKING

Maximum Power Point Tracking (MPPT) is an advantageous instrument in photovoltaic applications. The primary determinants affecting the electricity produced by a photovoltaic system are sun radiation and temperature. The voltage at which a photovoltaic module generates maximum power is termed the "maximum power point" (MPP). The primary principle of MPPT is extracting the maximum feasible power from solar energy and delivering it to the load using a dcto-dc converter that adjusts the voltage to the required level [5]. The operating point of a PV generator is located at the intersection of its current-voltage curve and the load line. The operating point may be far from the generator's maximum power point (MPP), resulting in significant wastage of available solar energy. An MPP tracker, often including a fundamental dc-dc converter, is used to achieve optimum alignment between the photovoltaic generator and the load. An MPPT algorithm regulates the duty cycle of the converter to optimize the power delivered to the load.

Copyright to IJARSCT www.ijarsct.co.in







International Journal of Advanced Research in Science, Communication and Technology

SOUTH SOUTH STATE OF THE SOUTH SOUTH

International Open-Access, Double-Blind, Peer-Reviewed, Refereed, Multidisciplinary Online Journal

Volume 5, Issue 1, October 2025

Impact Factor: 7.67

Numerous MPPT methods, such as the P&O algorithm, have been proposed [1-3]. This fundamental approach, which is simple to use, requires no previous knowledge of photovoltaic generator parameters or measurements of solar irradiance and cell temperature. The approach adjusts the operating point by altering a control parameter slightly and then compares the output power of the PV array before and after the modification. If the power increases, the algorithm perpetuates disruption in the same direction; otherwise, the approach alters the system in the other direction.

The P&O methodology is typically executed using two approaches: reference voltage perturbation [4-10] and direct duty ratio perturbation [5, 7, 11-13]. The output voltage reference of the PV array is used as a control parameter alongside a controller (often a PI controller) to modulate the duty cycle of the MPPT power converter for reference voltage perturbation. The gains of the PI controller are optimized when the system operates at a constant voltage corresponding to the standard test condition (STC) of the maximum power point (MPP) voltage. The MPPT algorithm regulates the reference voltage while maintaining steady gains. The duty ratio of the MPPT converter is used directly as the control parameter for direct duty ratio perturbation.

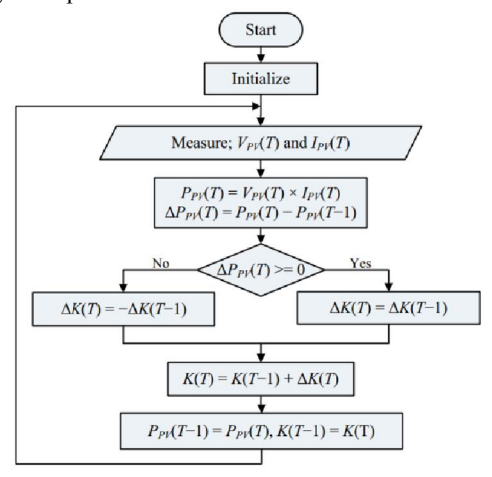


Fig 2:Flowchart of P&O MPPT algorithm

A. ZETA CONVERTER:

A zeta converter is a fourth order converter. Nonlinear system in the sense that it may be seen as a buck-boost-buck converter for energy input and a boost-buck-boost converter for output. The optimum switch-based zeta converter implementation is shown. Figure 3 depicts a non-isolated zeta converter circuit. While this converter may operate in a variety of modes depending on inductance value, load resistance, and operation frequency, only continuous inductor current "iL1" is examined here using the well-known state-space averaging approach. The following assumptions are used in the analysis.

Semiconductors switching devices are regarded as ideal.

The converter is in continuous inductor current mode.

•The line frequency ripple in the dc voltage is ignored.

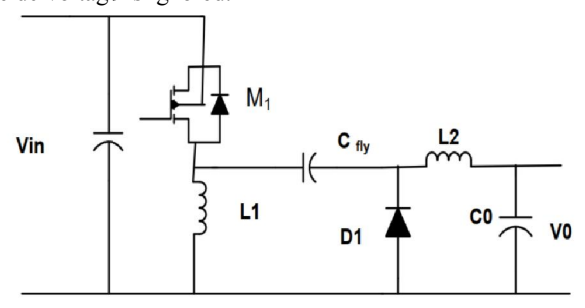


Fig 3: Proposed Structure of Basic Zeta converter







International Journal of Advanced Research in Science, Communication and Technology

Technology 9001:201

International Open-Access, Double-Blind, Peer-Reviewed, Refereed, Multidisciplinary Online Journal

Volume 5, Issue 1, October 2025

Impact Factor: 7.67

B. PRINCIPLE OF OPERATION:

When analysing Zeta converter, its waveform shows the equilibrium, L_1 average current equals I_{IN} and L_2 average current equals I_{out} since there is no DC current through the flying capacitor C_{FLY} . Also, there Stage-1[M_1 ON]

The switch M1 is in ON state, so voltages VL_1 and VL_2 are equal to Vin . In this time interval diode D1 is OFF with a reverse voltage equal to - $(V_{in} + V_o)$. Inductor L_1 and L_2 get energy from the voltage source, and their respective currents IL_1 and IL_2 are increased linearly by ratio V_{in}/L_1 and V_{in}/L_2 respectively. Consequently, the switch current IM1= IL_1 + IL_2 is increased linearly by a ratio Vin/L, where $L=L_1.L_2/(L_1+L_2)$. At this moment, discharging of capacitor C fly and charging of capacitor C0 take place.

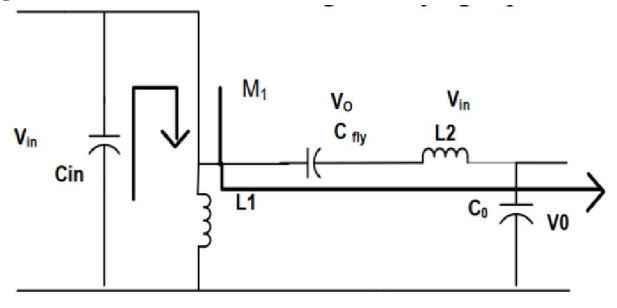


Fig 4: Zeta converter during MOSFET ON time

Stage-2 $[M_1 \text{ OFF}]$

Is no DC voltage across either inductor. Therefore, C_{FLY} ground potential at its left side and V_{OUT} at its right side, resulting the DC voltage across C_{FLY} is equal to VOUT.

In this stage, the switch M_1 turns OFF and the diode D_1 is forward biased starting to conduct. The voltage across L_1 and L_2 become equal to $-V_o$ and inductors L_1 and L_2 transfer energy to capacitor C_{fly} and load respectively. The current of L_1 and L_2 decreases linearly now by a ratio $-V_o/L1$ and $-V_o/L2$, respectively. The current in the diode $ID_1=IL_1+IL_2$ also decreases linearly by ratio $-V_0/L$. At this moment, the voltage across switch M1 is $V_M=V_{in}+V_o$.

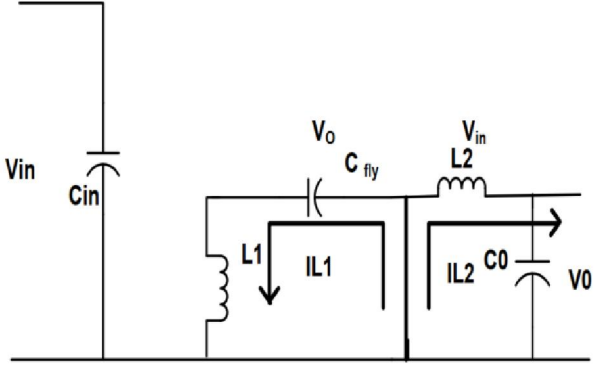


Fig 5:Zeta converter during MOSFET OFF time

IV. CONTROL STRATEGY OF PROPOSED SYSTEM

The control of the proposed drive system is split into two parts: MPPT control in the front-end converter and load-end VSI control for optimum motor electronic commutation during driving and regenerative mode. In the preceding section, we discussed the MPPT control approach. As a result, the sensor-free electronic commutation approach of the PMBLDC motor with regenerative braking is thoroughly investigated here.

Electronic Commutation

The six-step electronic commutation of the PMBLDC motor is done by accurate switching of the VSI in 120-degree mode of operation using three virtual Hall sensor signals generated by the sensor less control algorithm. Two power







International Journal of Advanced Research in Science, Communication and Technology

ISO 9001:2015

International Open-Access, Double-Blind, Peer-Reviewed, Refereed, Multidisciplinary Online Journal

Volume 5, Issue 1, October 2025

Impact Factor: 7.67

switches are engaged at the same time on each 60-degree step. As a consequence, two phases of the motor are active at each commutation period, while the other phase remains quiet.

DuVSI is used as a single-phase rectifier in PWM mode to charge the battery during ring regenerative braking. Table I shows the VSI switching procedure for both types of operation.

TABLE I. SWITCHING STATES OF THE VSI

Steps	0°-60°	60°-	120°-	180°-	240°-	300°-
Mode		120°	180°	240°	300°	360°
Motor	S1. S4	S1. S6	S3. S6	S3. S2	S5. S2	S5. S4
Regen.	S3. S2	S5. S2	S5. S4	S1. S4	S1. S6	S3. S6

Control Topology

The third harmonic stator flux is used here to allow electrical commutation of the motor without the need of a position sensor. The third harmonic flux is calculated using the motor's back emfs. The following is the Fourier series representation of the three phase back emfs:

$$\begin{split} e_{A} &= E_{1}sin\theta + E_{1}sin30 + E_{1}sin50 + \cdots \dots (1) \\ e_{B} &= E_{1}sin(\theta - \frac{2_{\pi}}{3}) + E_{1}sin3(\theta - \frac{2_{\pi}}{3}) + E_{1}sin5(\theta - \frac{2_{\pi}}{3}) + \cdots \dots (2) \\ e_{C} &= E_{1}sin\left(\theta - \frac{4_{\pi}}{3}\right) + E_{1}sin3\left(\theta - \frac{4_{\pi}}{3}\right) + E_{1}sin5\left(\theta - \frac{4_{\pi}}{3}\right) + \cdots \dots (3) \end{split}$$

Where θ is the electrical rotor angle. The sum of the three back-emf equations is expressed as,

$$e_A + e_B + e_C = 3E_3 \sin 3\theta + 3E_9 \sin 9\theta + E_{15} \sin 15\theta + \approx 3E_3 \sin 3\theta$$
 (4)

Again, the total of the PMBLDC motor's three phase voltages is used,

$$u_{sum} = u_{an} + u_{bn} + u_{cn}$$

$$\left(Ri_A + L\frac{d}{dt}\right)(i_A + i_B + i_c) + (e_A + e_B + e_C)(5)$$

As in steady state, $(i_A + i_B + i_c) = 0$,

 u_{sum} can be approximated as,

$$u_{sum} = e_A + e_B + e_C \approx 3E_3 \sin 3\theta \tag{6}$$

As a result of (4) and (6), it is possible to conclude that information about the third harmonic component of backemf is encoded in the sum of three phase voltages.

Now third harmonic stator flux can be obtained as,

$$\Psi_{3rd} = \int u_{sum} dt \, dt \qquad (7)$$

As illustrated in Fig. 6, the generated third harmonic stator flux linkage from the integration of the u sum may be utilised to estimate the location of the rotor since the zero-crossing points of _3rd are the precise commutation points.

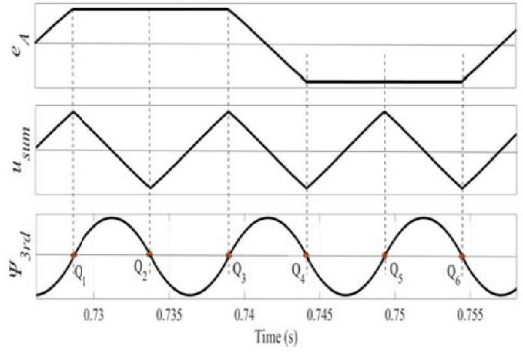


Fig 6: Relationship among back-emf and stator flux and zero-crossings

Copyright to IJARSCT www.ijarsct.co.in







International Journal of Advanced Research in Science, Communication and Technology

ommunication and Technology

Impact Factor: 7.67

International Open-Access, Double-Blind, Peer-Reviewed, Refereed, Multidisciplinary Online Journal

Volume 5, Issue 1, October 2025

Elimination of false zero-crossings

The three back-emf signals are generated using the motor's terminal voltage. The observed terminal voltages in Fig. 7 exhibit unwanted spikes. This results in erroneous zero crossings and causes the VSI's whole switching logic to fail. A first order lowpass filter is designed to remove those annoying spikes.

The cut off frequency must be carefully chosen while creating the filter. Taking phase lag into account, the cut off frequency in this study is set at 1000 rad/s. The lowpass filter's transfer function is,

$$H(s) = \frac{\omega_c}{s + \omega_c} = \frac{1000}{s + 1000}$$
 (8)

The LPF adds some phase lag to the system. The phase lag in relation to the speed of the PMBLDC motor may be calculated as,

$$\emptyset = -tan^{-1}\frac{\omega}{\omega_c} = -tan^{-1}\left(\frac{2\pi \times 33.33}{1000}\right) = -11.7^{\circ}$$
 (9)

Where the angular frequency of the derived back-emf is denoted by. The phase lag induced by the LPF while running at 1200 rpm is -11.7o, as illustrated in Fig 8.

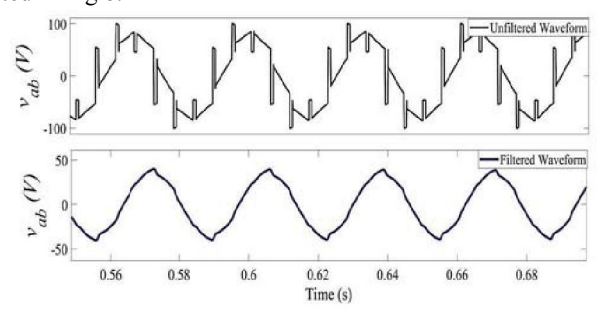


Fig 7: Unfiltered and filtered line voltage waveform

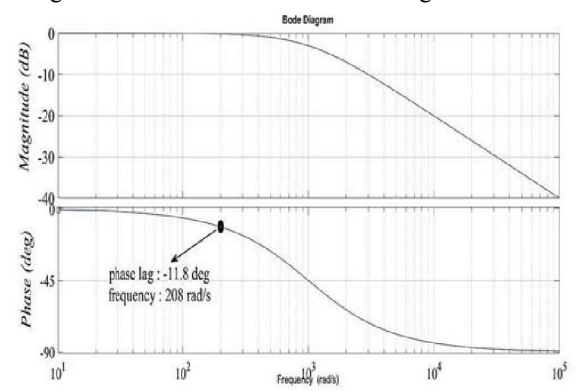


Fig 8: Bode plot diagram for lag compensator

Design Procedures of Lead Compensator

The phase lag generated by the lowpass filter causes mistakes in estimating the zero-crossing locations at greater speeds. Additionally, the torque ripple rises, potentially leading to considerable losses in the motor winding. As a consequence, to compensate for the additional lag, a compensator with a leading phase angle is necessary.

The lead compensator in this work is meant to correct for a phase lag of -11.80 at a frequency of 208.4 rad/s while the motor is operating at 1200 rpm. The compensator transfer function is expressed as follows,

$$G(s) = k \frac{s + \omega_{c1}}{s + \omega_{c2}} \tag{10}$$

Where k is the magnitude constant and c1 and c2 are the zero and pole crossover frequencies, respectively. The predicted value of k is,

Copyright to IJARSCT www.ijarsct.co.in









International Journal of Advanced Research in Science, Communication and Technology

International Open-Access, Double-Blind, Peer-Reviewed, Refereed, Multidisciplinary Online Journal

Volume 5, Issue 1, October 2025

Impact Factor: 7.67

$$k = \frac{1 + \sin \theta}{1 - \sin \theta} = \frac{1 + \sin 11.8}{1 - \sin 11.8} = 1.51$$

The time constant T is,

$$T = \frac{1}{\omega \times \sqrt{k}} = \frac{1}{208.4 \times \sqrt{1.51}} = 3.90 \times 10^{-3} \, rad/s$$
 (12)

So, the cut off frequencies are estimated as,

$$\omega_{c1} = \frac{1}{kT} = \frac{1}{1.51 \times 3.90 \times 10^{-3}} = 169.80 \, rad/s \tag{13}$$

$$\omega_{c1} = \frac{1}{kT} = \frac{1}{1.51 \times 3.90 \times 10^{-3}} = 169.80 \, rad/s$$

$$\omega_{c1} = \frac{1}{kT} = \frac{1}{1.51 \times 3.90 \times 10^{-3}} = 256.41 \, rad/s$$
(13)

So, the transfer function becomes,

$$G(s) = k \frac{s + 169.80}{s + 256.41}$$
 (15)

The Bode plot for the aforementioned system is shown in Fig. 9. At frequency 208 rad/s, a phase lead of 11.80 is effectively achieved. Figure 7 shows the filtered waveform of the terminal voltage, which has been filtered to remove any undesired spikes. With these filtered and rectified waveforms, the commutation error of the PMBLDC motor may be considerably decreased.

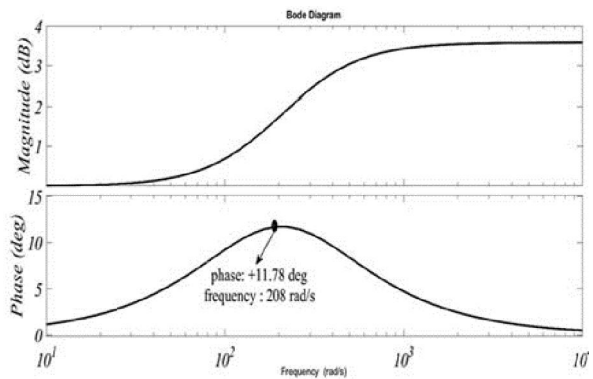


Fig 9: Bode plot diagram for lead compensator

V. RESULTS AND DISCUSSION

SIMULATION AND RESULTS

The complete EV model is simulated in MATLAB, the detailed simulation results along with discussions as follows. Performance of solar PV array

Performance of Zeta Converter

Performance of PMBLDC motor

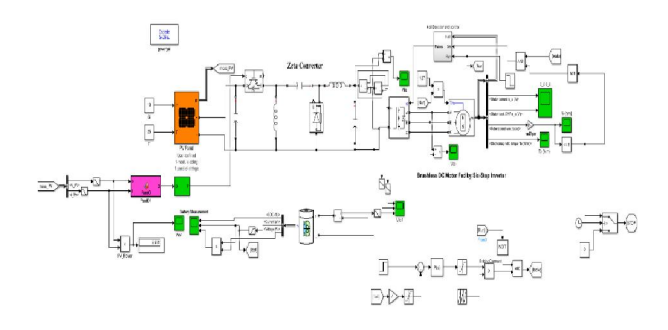


Fig 10: Simulink Model of the PV battery fed EV system with regenerative braking employing zeta converter





International Journal of Advanced Research in Science, Communication and Technology



International Open-Access, Double-Blind, Peer-Reviewed, Refereed, Multidisciplinary Online Journal

Volume 5, Issue 1, October 2025

Impact Factor: 7.67

To analyse the performance of the solar PV battery fed ev system with regenerative braking employing zeta converter. The PV parameters of the system are shown in Table II.

TABLE II: PV PARAMETERS

Parameters	Specifications	
Maximum power (W)	334.905 W	
Parallel strings	1	
Series-connected modules per string	1	
Cells per module (Ncell)	80	
Open circuit voltage Voc (V)	49.9	
Short-circuit current Isc (A)	9	
Voltage at maximum power point Vmp (V)	41.5	
Current at maximum power point Imp (A)	8.07	

Performance evaluation of a solar PV battery-fed electric vehicle with regenerative braking using a zeta converter at 1000 IR and 25 Degree Temp, Solar (PV) and Battery Both the source are used while testing the proposed system. Figures 12, 15, 20 and 23 show results for regenerative braking at 0.5 sec; when braking was applied, torque and speed went negative, and the battery started charging via regenerative braking.

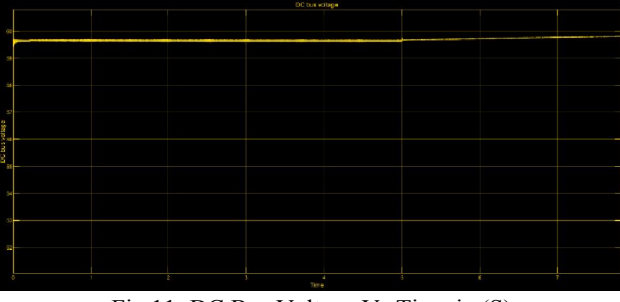


Fig 11: DC Bus Voltage Vs Time in (S)

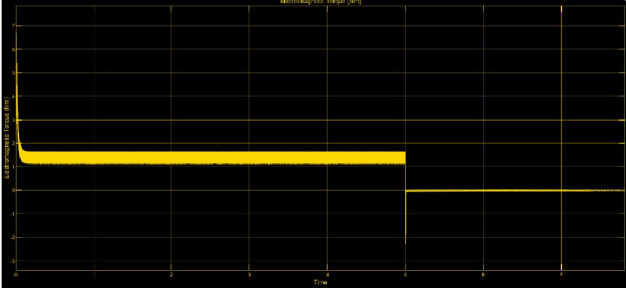


Fig 12: Electromagnetic Torque (NM) of BLDC Motor Vs Time in (S)

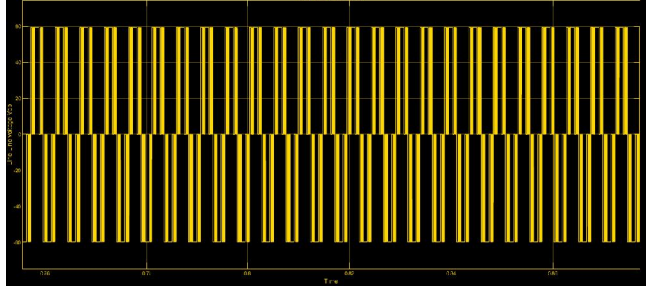


Fig 13: Line – Line Voltage (Vab) Vs Time in (S)





International Journal of Advanced Research in Science, Communication and Technology

ISO 9001:2015

International Open-Access, Double-Blind, Peer-Reviewed, Refereed, Multidisciplinary Online Journal

Volume 5, Issue 1, October 2025



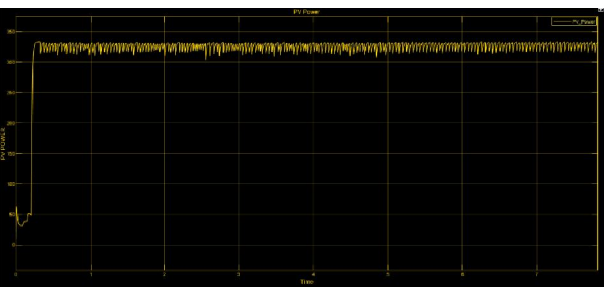


Figure 14. PV Power Vs Time in (S)

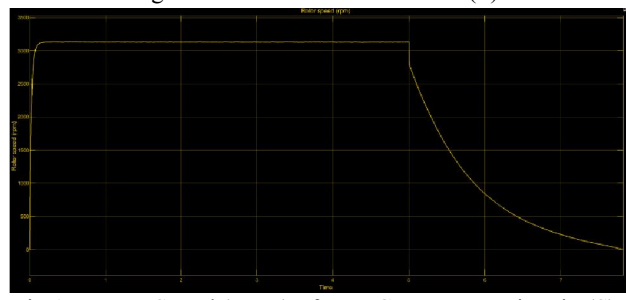


Fig 15: Rotor Speed (RPM) of BLDC Motor Vs Time in (S)

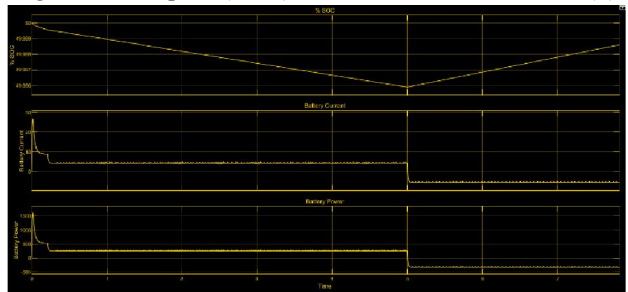


Fig 16: SOC %, Battery Current and Battery Power Vs Time in (S)

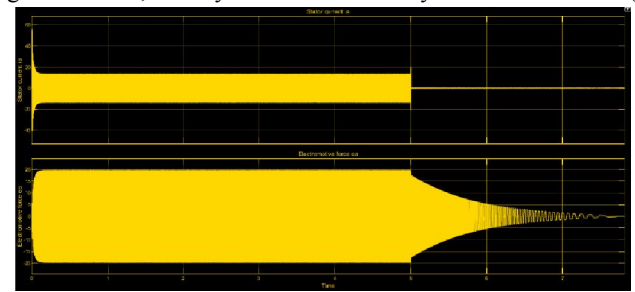


Fig 17: Stator Current Ia and Electromotive Force Ea Vs Time in (S)

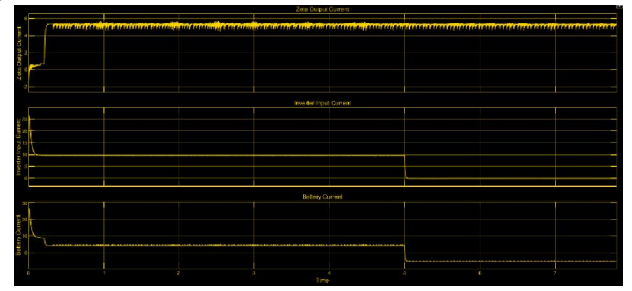


Fig 18: Zeta Converter Output Current, Inverter Input Current and Battery Current Vs Time in (S)





International Journal of Advanced Research in Science, Communication and Technology

ISO 9001:2015

International Open-Access, Double-Blind, Peer-Reviewed, Refereed, Multidisciplinary Online Journal

Volume 5, Issue 1, October 2025

Impact Factor: 7.67

Performance evaluation of a solar PV battery-fed electric vehicle with regenerative braking using a zeta converter at 10 IR and 25 Degree Temp, PV power is zero, so battery power is the only source used while testing the proposed system.

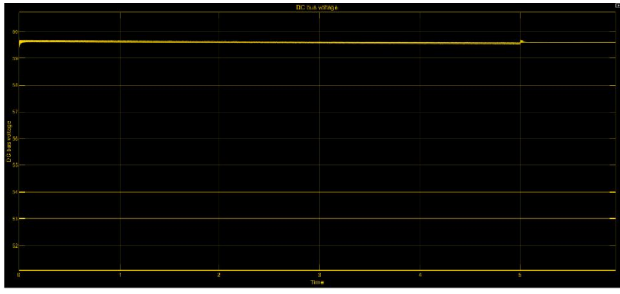


Fig 19: DC Bus Voltage Vs Time in (S)

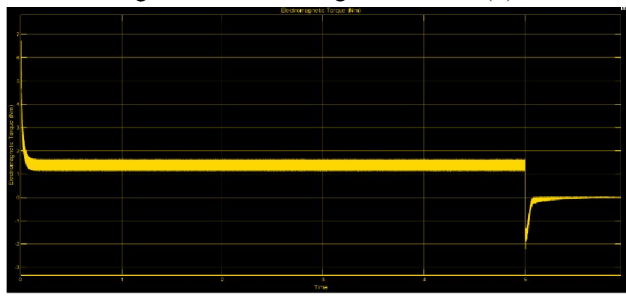


Fig 20: Electromagnetic Torque (NM) of BLDC Motor Vs Time in (S)

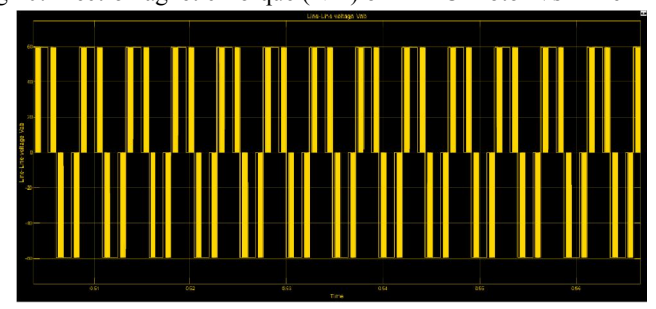


Fig 21: Line – Line Voltage (Vab) Vs Time in (S)

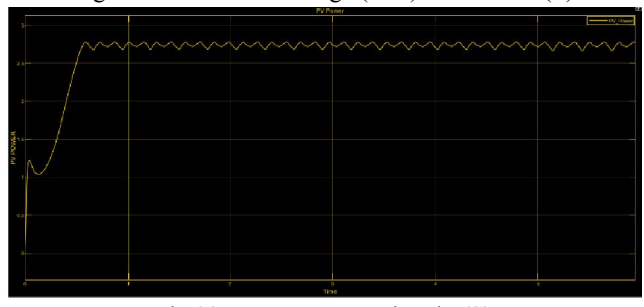


Fig 22: PV Power Vs Time in (S)





International Journal of Advanced Research in Science, Communication and Technology

ISO 9001:2015

International Open-Access, Double-Blind, Peer-Reviewed, Refereed, Multidisciplinary Online Journal

Volume 5, Issue 1, October 2025



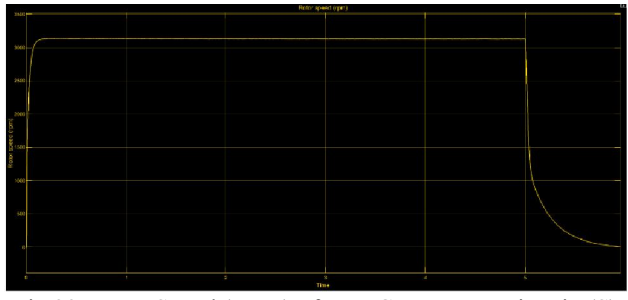


Fig 23: Rotor Speed (RPM) of BLDC Motor Vs Time in (S)

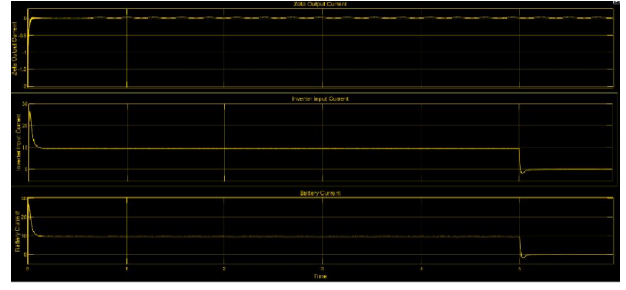


Fig 24: SOC %, Battery Current and Battery Power Vs Time in (S)

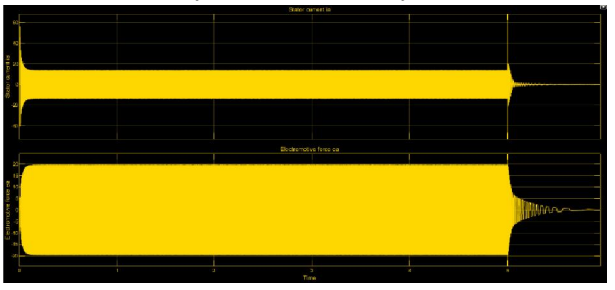


Fig 25: Stator Current Ia and Electromotive Force Ea Vs Time in (S)

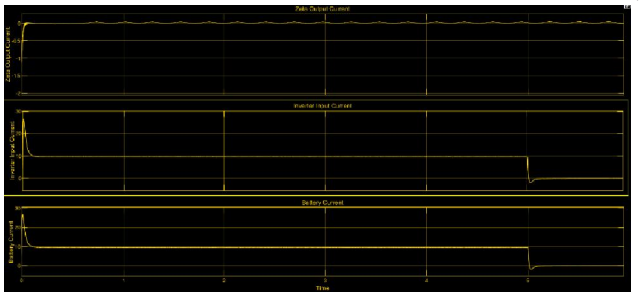


Fig 26: Zeta Converter Output Current, Inverter Input Current and Battery Current Vs Time in (S)

VI. CONCLUSION

This paper describes an electric vehicle power train with regenerative braking technology and speed control of a PMBLDC motor driven by a solar-PV and battery system. The speed is managed online based on the peak power of the solar-PV panel and the load requirement. The battery is charged by the vehicle's kinetic energy during braking, allowing regeneration to occur. The intermediary DC-DC converter step is removed during this operation. A noninverted zeta converter with constant output current provides effective MPPT control of a solar-PV array. The VSI switches are gated at fundamental frequency, which reduces the losses associated from high-frequency switching. In terms of stability and controllability, the developed system is supposed to be robust.

Copyright to IJARSCT www.ijarsct.co.in



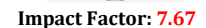




International Journal of Advanced Research in Science, Communication and Technology

International Open-Access, Double-Blind, Peer-Reviewed, Refereed, Multidisciplinary Online Journal

Volume 5, Issue 1, October 2025



REFERENCES

- [1]. Valentin Totev; VultchanGueorgiev "Efficiency of Regenerative Braking in Electric Vehicles" 2020 21st International Symposium on Electrical Apparatus & Technologies (SIELA).
- [2]. Abhishek Gaurav; Anurag Gaur "Modelling of Hybrid Electric Vehicle Charger and Study the Simulation Results" 2020 International Conference on Emerging Frontiers in Electrical and Electronic Technologies (ICEFEET).
- [3]. Dragos Niculae;MihaiIordache;MarilenaStanculescu;Maria Lavinia Bobaru;SorinDeleanu "A Review of Electric Vehicles Charging Technologies Stationary and Dynamic" 2019 11th International Symposium on Advanced Topics in Electrical Engineering (ATEE).
- [4]. AhadJavandoustQarebagh;FarnazSabahi;Dariush "NazarpourOptimized Scheduling for Solving Position Allocation Problem in Electric Vehicle Charging Stations" 2019 27th Iranian Conference on Electrical Engineering (ICEE).
- [5]. JunbeomWi;HyunhwaKim;JihoYoo;HanhoSon;HyunsooKim;Byungjae Kim "Energy consumption of parallel type hybrid electric vehicle with continuously variable transmission using electric oil pump" 2018 Thirteenth International Conference on Ecological Vehicles and Renewable Energies (EVER).
- [6]. ChaoqunLiu;BinWei;SongcenWang;XiaokangWu;XianZhang;JieWang;Qingxin Yang "Field Circuit Coupling Analysis of Dynamic Wireless Charging for Electric Vehicle" 2018 IEEE 2nd International Electrical and Energy Conference (CIEEC).
- [7]. Jing Zhang;HuiYan;NingDing;JianZhang;TaoyongLi;ShuSu "Electric Vehicle Charging Network Development Characteristics and Policy Suggestions" 2018 International Symposium on Computer, Consumer and Control (IS3C).
- [8]. ArazSaleki;SamanRezazade;MahmudrezaChangizian "Analysis and simulation of hybrid electric vehicles for sedan vehicle" 2017 Iranian Conference on Electrical Engineering (ICEE).
- [9]. V. P. Dhote; M. M. Lokhande; Akash Agrawal; B. Hemanth Kumar "Mechanical coupling of two induction motor drives for the applications of an electric-drive vehicle system" 2017 National Power Electronics Conference (NPEC).
- [10]. Oliver Marcincin; Zdenek Medvec; Petr Moldrik "The impact of electric vehicles on distribution network" 2017 18th International Scientific Conference on Electric Power Engineering (EPE).
- [11]. Fatemeh Jozi; KazemMazlumi; Hadi Hosseini "Charging and discharging coordination of electric vehicles in a parking lot considering the limitation of power exchange with the distribution system" 2017 IEEE 4th International Conference on Knowledge-Based Engineering and Innovation (KBEI).
- [12]. EgorKulik;XuanTrungTran;AleckseyAnuchin;YuriyVagapov "GPS-track data processing for the optimization of the powertrain for hybrid electric vehicles" 2017 IEEE 58th International Scientific Conference on Power and Electrical Engineering of Riga Technical University (RTUCON).
- [13]. SomayyehKhatiri-Doost; MeysamAmirahmadi "Peak shaving and power losses minimization by coordination of plug-in electric vehicles charging and discharging in smart grids" 2017 IEEE International Conference on Environment and Electrical Engineering and 2017 IEEE Industrial and Commercial Power Systems Europe (EEEIC / I&CPS Europe).
- [14]. X. D. Xue; K. W. E. Cheng; S. Raghu Raman; Jones Chan; J. Mei; C. D. Xu "Performance prediction of light electric vehicles powered by body-integrated super-capacitors" 2016 International Conference on Electrical Systems for Aircraft, Railway, Ship Propulsion and Road Vehicles & International Transportation Electrification Conference (ESARS-ITEC).
- [15]. Muhammad SifatulAlamChowdhury; Khandakar Abdulla Al Mamun; Al Mahmudur Rahman" Modelling and simulation of power system of battery, solar and fuel cell powered Hybrid Electric vehicle" 2016 3rd International Conference on Electrical Engineering and Information Communication Technology (ICEEICT)

